한국정밀공학회지 제 42 권 제 4 호 pp. 333-345 April 2025 / 333
J. Korean Soc. Precis. Eng., Vol. 42, No. 4, pp. 333-345 http://doi.org/10.7736/JKSPE.025.015
ISSN 1225-9071 (Print) / 2287-8769 (Online)

LDPE 고분자에서의 가스 충전량과 확산도 측정을 위한 부피 분석과 압력 분석에 기반한 가스 센서 개발

Development of Gas Sensors based on Volumetric and Manometric Analysis for Measuring Gas Emission and Diffusion Coefficient in Low-density Polyethylene Polymer

이지훈[1,#], 전상구[1]
Ji Hun Lee[1,#] and Sang Koo Jeon[1]

1 한국표준과학연구원 수소에너지그룹 (Hydrogen Energy Group, Korea Research Institute of Standards and Science)
Corresponding Author / E-mail: ljh93@kriss.re.kr, TEL: ※ 개인정보 표시제한
ORCID: 0000-0002-8120-638X

KEYWORDS: Gas sensors (가스 센서), Volumetric measurement (부피측정법), Manometric measurement (압력측정법), Gas uptake (가스 장입량), Diffusion (확산)

Gas sensors are crucial devices in various fields such as industrial safety, environmental monitoring, and gas infrastructure. Designed to have high-sensitivity, stability, and reliability, gas sensors are often required to be cost-effective with quick response and compactness. To meet diverse needs, we developed two types of gas sensors based on volumetric and manometric analyses. These sensors could operate by measuring gas volume and pressure changes, respectively, based on emitted gas. These sensors are capable of determining gas transport parameters such as gas uptake, solubility, and diffusivity for gas-charged polymers in a high-pressure environment. These sensors can provide rapid responses within one-second. They can measure gas concentration ranging from 0.01 wt·ppm to 1,500 wt·ppm with adjustable sensitivity and measurement ranges. As a result, such sensor system can be used to facilitate real time detection and analysis of gas transport properties in pure gases including H_2, He, N_2, O_2, and Ar.

Manuscript received: February 4, 2025 /Accepted: March 13, 2025

1. Introduction

Gas detecting sensor is crucial for ensuring safety, particularly under environments where hazardous gases like hydrogen or carbon monoxide are released [1-10]. Early detection of gas emission and leak can prevent accidents, fires and risks. It is also essential for environmental monitoring, as it helps in detecting pollutants and maintaining air quality. Accurate gas sensing plays an important role in optimizing operations, particularly for renewable energy source like hydrogen. By ensuring precise monitoring of hydrogen gas concentrations, it enhances safety, efficiency and performance throughout the hydrogen production, storage and distribution processes [11-22].

In hydrogen refueling station charged to high-pressure H_2, polymer materials play an important role [23-45]. For instance, polymer-based materials such as O-ring seals, gasket, liner material and non-metallic pipeline are widely used. It was designed to withstand hydrogen environments. However, these polymers are subjected to harsh conditions including wide temperature fluctuations (-70 to 90ºC) and pressure variations (1 to 90 MPa). These conditions can lead to seal damage, insufficient contact with glove and gas permeation through polymer seals, all of which can result in hydrogen leakage [46-52].

Gas permeation including hydrogen in polymer materials also

occurs when gases pass through the polymer matrix due to diffusion. This process is influenced by aspects including temperature, pressure and chemical natures of both the gas and the polymer [53-55]. For instance, in the use of polymer membranes for gas separation, materials like polyimide are employed to selectively permeate gases like oxygen or carbon dioxide while blocking other gases. A common example is the use of polymeric membranes in CO_2 capture systems, where the membrane's permeability to CO_2 is crucial for effective separation from industrial emissions. However, the permeation rate can vary based on the polymer's structure, with amorphous polymers typically having higher permeability compared to crystalline ones. Gas permeation is a key consideration in applications like gas storage and delivery, where polymers need to have low gas diffusion/permeability to avoid leakage and maintain system integrity.

Meanwhile, gas sensors are vital for accurately detecting specific gas concentration and leakage across applications where gas is produced, stored and used, such as fuel cells, storage facilities and transportation systems [56,57]. These gas sensors are developed based on different sensing principles, each with its own advantages and limitations. Infrared (IR) gas sensing [58-60] works on the principle that gas molecules absorb infrared light at specific wavelengths. The intensity of absorbed light is measured and correlated to concentration of the corresponding gas. The main advantages of IR gas sensing include high sensitivity, selectivity and ability to detect gases over a wide range of concentrations. However, it could be affected by environmental conditions including temperature and humidity and may require regular calibration for accurate measurements.

Semiconductor gas sensors [61-63] operate based on the principle that gas molecules interact with the surface of a semiconductor material (Typically Metal Oxides), causing a change in its electrical resistance. The change in resistance is measured and intercorrelated to the concentrations of the target gas. The advantages include low cost, fast response and small size. However, they can be influenced by factors like temperature, pressure and humidity and may exhibit cross-sensitivity to other gases, reducing accuracy.

Catalytic combustion gas sensors [64-66] operate by detecting gases through the catalytic oxidation of the target gas on a heated catalyst surface, which generates heat. This heat change is measured and used to determine the gas concentration. The advantages include high sensitivity to combustible gases and reliability in detecting flammable gases at low concentrations. However, they have a limited lifespan, especially in the presence of poisons like silicone or lead. The sensors may require regular maintenance to ensure the accurate performance.

An optical spectroscopy gas sensor [67-69] operates based on the principle that gas molecules absorb or emit light at specific wavelengths. When light passes through a gas sample or is reflected from it, the gas molecules absorb light at characteristic absorption bands corresponding to their molecular structure. The amount of absorbed light is then measured, which is correlated to concentrations of the gas. Key features of optical spectroscopy gas sensors include high sensitivity, non-destructive measurement and ability to detect low concentrations of gases with high accuracy. These sensors are capable of detecting wide ranges of gases and are immune to interference from most other substances. However, they may be affected by environmental factors like temperature, pressure and the presence of other gases in complex mixtures.

An electrochemical gas sensor [70-72] operates by detecting gases through a chemical reaction between the target gas and the electrodes in an electrolyte. This reaction produces electrical currents proportional to concentrations of the gas, which is then measured and used to determine the gas level. The advantages of electrochemical sensors include high sensitivity, low power consumption, and good selectivity for specific gases. However, they could be influenced by factors like temperature and humidity and their lifespan may be limited due to the degradation of the electrodes or electrolyte over time.

Finally, gas chromatography [73-79] and mass spectrometry [80-82] provide highly precise analysis and commonly used in research and laboratory settings. Gas chromatography separates and analyzes individual components in gas mixtures, while mass spectrometry identifies gas molecules based on their mass after ionization. However, these sensing systems are expensive and require regular maintenance, making them unsuitable for real-time field monitoring.

The conventional gas sensing technologies provide precise measurements but face challenges in specimen size, sensitivity, selectivity and environmental stability. These limitations highlight the need for advanced gas sensors that are compact, have rapid response times, high sensitivity and robust performance across variable field conditions to ensure safety in real-time gas monitoring.

Thus, we have developed two types of gas sensors with the performance to meet these requirements. First, a sensor system utilizing a volumetric measurement (VM) method based on the image processing algorithm is developed [5,83]. This system aims to provide the real-time monitoring by connecting to a computer via a GPIB interface and using a diffusion analysis program to accurately measure gas concentration/diffusion in the polymer specimen with the insensitivity to temperature/pressure changes.

Second, a simple and effective gas detection sensor based on a

manometric measurement (MM) method was developed using the portable data logger with USB type to measure and record pressure/temperature in a sample container and a diffusion analysis program [84-86]. This portable detection system can easily measure gas concentration and diffusion from the polymer samples in real-time on-site without any chemical interactions with gas.

It was demonstrated that the developed two gas sensor systems have the versatility to detect and characterize various gases like H_2, He, N_2, O_2, and Ar, effectively sensing gas adsorption and diffusion in polymer materials in real-time. The sensor has shown reliable performance in sensitivity, stability and response time. The sensor technology presented in this study offers a compact and portable solution capable of replacing large-scale equipment. It has potential applications not only in hydrogen infrastructure safety management but also in the gas industry for real time gas monitoring. We compare the principles, procedures, results and characteristics of each method. Ultimately, two developed gas sensing methods provide valuable insights into the gas transport properties, leakage and sealing capabilities of O-rings under high-pressure conditions. They are applicable in hydrogen fueling stations and the gas industry, enhancing safety and enabling real-time monitoring.

2. Experimental Procedure

2.1 Specimen Preparation and High-pressure Gas Charging

This developed gas sensor is applied to measure gas concentration and diffusion coefficient from polymer specimen during the desorption process of gas charged to high pressure. Polymer specimen used is low-density polyethylene (LDPE). LDPE is widely used for manufacturing containers and gas transport pipes. It is known as its gas-barrier properties when coated. LDPE is used as an O-ring seal material in high-pressure gas chambers. The developed gas detection system allowed us to determine the permeation properties (Solubility, Diffusion Coefficient and Permeability) of polymer samples.

The composition and density details of the polymer sample can be found in prior literatures [3,86]. The polymer sample were prepared with the following cylinderical shapes and dimensions:

- LDPE : radius (R) 9.51, thickness (T) 4.89 and 1.57 mm

For high-pressure gas charging, we used a stainless steel 316 chamber at room temperature and desired pressure conditions. Gas charging was conducted at pressure of 5 MPa. The purity of the gases used was as:

- H_2: 99.99%, He: 99.99%, N_2: 99.99%, O_2: 99.99%, Ar: 99.99%

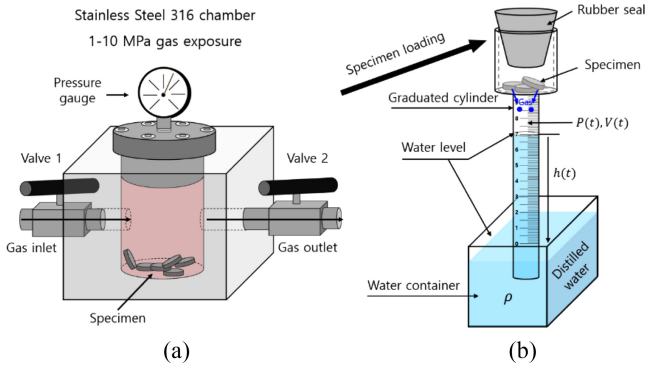

Fig. 1 Volumetric sensor system to measure the gas uptake and diffusivity emitted by a specimen after charging to HP gas. (a) Specimen charged to gas in a HP chamber. (b) After decompression in the chamber, the specimen was loaded into a graduated cylinder. The cylinder was partially immersed in a water container and gas emission measurements were performed. The ● in cylinder represents the gas emitted from the charged sample

Samples were then charged to the gas at the specified pressure for 24-48 hours. A 48 hours gas charging was sufficient to reach the equilibrium for gas absorption into specimen.

2.2 Volumetric Measurement of the Released Gas from Charged Polymers

A volumetric measurement technique to assess gas diffusion and permeation is developed. This method involves measuring the concentration of gas released from a specimen after charging to high pressure (HP) and decompression. Fig. 1 illustrates a volumetric analysis system used to quantify the released gas at a room temperature. The system consists of a high-pressure chamber for gas charging and a cylinder immersed in a water container.

After charging to high-pressure gas and decompression, the specimen was placed in the upper air space of a graduated cylinder, as depicted in Fig. 1. The gas released from the specimen caused a gradual decrease in the water level within the cylinder. Consequently, the pressure (P) and volume (V) of the gas inside the cylinder varied with time.

The gas within the cylinder adheres to the ideal gas law, expressed as PV = nRT, where R is the gas constant (8.20544×10^{-5} $m^3 \cdot atm/(mol \cdot K)$), T represents the gas temperature inside the cylinder, and n denotes the number of moles of gas released into the cylinder. The variations of pressure P(t) and volume V(t) of the gas in the cylinder can be described as follows [87]:

$$P(t) = P_o(t) - \rho g h(t),\ V(t) = V_o - V_s - V_h(t) \quad (1)$$

where P_o represents the external pressure surrounding the cylinder, g is the gravitation acceleration, and ρ signifies the density of dis-

tilled water. The $h(t)$ describes the water level within the cylinder over time, while V_o is the combined volume of gas and water inside the cylinder, measured relative to the water level in the container. $V_h(t)$ indicates the time-dependent volume of water in the cylinder, and V_s represents the volume occupied by the sample. The amount of gas released by the polymer specimen was quantified by tracking the water level position [$V_h(t)$] over time. Consequently, the total moles of gas emitted [$n(t)$] were calculated by measuring the total gas volume [$V(t)$] in the graduated cylinder, which corresponds to the decrease in the water level, as expressed by the following [87]:

$$n(t) = \frac{P(t)V(t)}{RT(t)} = \frac{P(t)[V_A + V_H(t)]}{RT(t)} = \frac{P_o[1+\beta(t)][V_A + V_H(t)]}{RT_0[1+\alpha(t)]}$$

$$\cong \frac{P_o}{RT_0}[V_A + V_H(t) + V(t)(\beta(t) - \alpha(t))] = n_A(t) + n_H(t)$$

$$\text{with } n_A(t) = \frac{P_o}{RT_0}V_A,$$

$$n_H(t) = \frac{P_o}{RT_0}[V_H(t) + V(t)(\beta(t) - \alpha(t))]$$

$$\alpha(t) = \frac{T(t) - T_0}{T_0},\ \beta(t) = \frac{P(t) - P_0}{P_0}, \quad (2)$$

Here, T_0 and P_0 represent the initial temperature and pressure of the gas in the cylinder, respectively. $V(t)$ is the total volume, consisting of the remaining initial air volume (V_A) and the released gas volume [$V_H(t)$], so that $V(t) = V_A + V_H(t)$. n_A denotes the initial mole number of air and $n_H(t)$ refers to the time-dependent mole number of gas corresponding to the increase in gas volume due to its release. Therefore, $n_H(t)$ was converted to the gas concentration, [$C(t)$] emitted per unit mass from the specimen as :

$$C(t)[\text{wt·ppm}] = n_H(t)[\text{mol}] \times \frac{m_{Gas}\left[\frac{\text{g}}{\text{mol}}\right]}{m_{sample}\left[\frac{\text{g}}{\text{mol}}\right]} \times 10^6$$

$$= \frac{P_o}{RT_0}[V_H(t) + V(t)(\beta(t) - \alpha(t))][\text{mol}] \times \frac{m_{H_2}\left[\frac{\text{g}}{\text{mol}}\right]}{m_{sample}[\text{g}]} \times 10^6 \quad (3)$$

For instance, the molar mass of hydrogen gas, m_{H_2} [g/mol] is 2.016 g/mol. The molar mass of nitrogen gas m_{N_2} [g/mol] is 28.013 g/mol. m_{sample} is the specimen mass. In Eqs. (2) and (3), the time-dependent mole number of gas, $n_H(t)$, was converted to the gas mass concentration, [$C(t)$], by the factor, $k = \left[\frac{m_{Gas}}{m_{sample}}\right]$. $n_H(t)$ and $C(t)$ are affected by the fluctuations of temperature and pressure in the laboratory environments. To ensure precise measurements, it's essential to compensate for these variations. This compensation can be achieved through automated programs according to Eq. (3). That is., the terms, $V(t)(\beta(t) - \alpha(t))$, indicates the volume change in the $V_H(t)$, caused by the temperature and pressure variations. The compensation indicates the application of $(t)(\beta(t) - \alpha(t))$ calculation in Eq. (3). Thus, the insensitivity of the sensor to variations in temperature and pressure means the application of automatic compensation by the program.

The release of gas was tracked by monitoring changes in water level measurement using image processing algorithm via digital camera in front of the graduated cylinder. The procedure for obtaining the water level (Emitted Gas Volume) from water level measurement is described in previous works [5,83].

2.3 Manometric Measurement of the Released Gas from Charged Polymers

Fig. 2 illustrates the schematic of the manometric measurement sequence used to determine the concentration and diffusivity of the released gas from specimen at 298 K. The setup includes a high-pressure chamber for the gas charging as shown in Figs. 2(a), a rectangular specimen container equipped with a commercial data logger with USB type and rubber seal in 2(b). The ELP sensors, which were used to measure pressure and temperature, are commercial data loggers capable of simultaneously recording both atmospheric pressure and temperature.

After the charging and decompression in the stainless steel chamber, the specimen was transferred into the rectangular specimen container shown in Fig. 2(b). As the gas realeased from the sample, the pressure inside the vessel increased with elapsed time. Consequently, both the pressure (P) and temperature (T) of the gas within the specimen container changed as time progressed. The gas inside the container followed the ideal gas law: $PV = nRT$, R is the gas constant with 8.20544×10^{-5} m³·atm/(mol·K), and n represents the number of moles of the released gas molecules inside the specimen container.

The mole number of gases emitted from charged specimen is obtained by measuring the increase in pressure [$P(t)$] versus time by manometric measurement at a constant container volume. Thus, the total number of moles [$n(t)$] obtained by measuring the increased gas pressure [$P(t)$] due to emitted gas in the cylindrical container is described as [3,86]:

$$n(t) = \frac{P(t)V_0}{RT(t)} = \frac{P(t)V_0}{RT(t)} = \frac{[P_0 + \Delta P(t)]V_0}{RT_0[1+\alpha(t)]}$$

$$\cong \frac{P_oV_0 + \Delta P(t)V_0}{RT_0}[1+\alpha(t)] = n_0 + \Delta t(t),$$

$$\text{with } n_0 = \frac{P_0V_0}{RT_0},$$

$$\Delta n(t) = \frac{V_0}{RT_0}[\Delta P(t) - \alpha(t)P_0 - \alpha(t)\Delta P(t)]$$

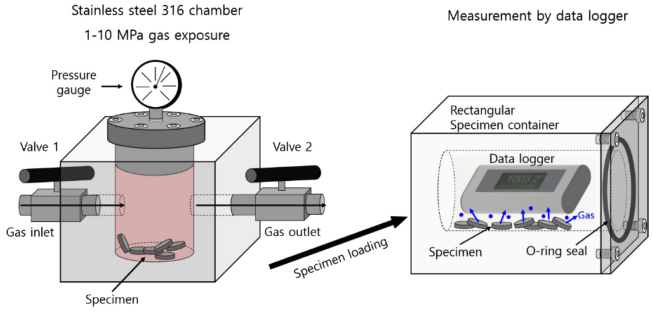

(a) (b)

Fig. 2 Illustration of manometric sensor system for measuring gas uptake and diffusion coefficient from charged sample using a commercial pressure/temperature logger after high-pressure charging and decompression. (a) The sample charged to gas in the high-pressure chamber. (b) After decompression of the chamber, the charged sample loaded in the rectangular specimen container. Gas emission measurements were carried out using a data logger within the sample container. The ● in specimen container represents the gas emitted from charged sample

$$\alpha(t) = \frac{T(t) - T_0}{T_0} \tag{4}$$

where T_0, V_0 and P_0 are the temperature, initial volume and initial pressure of the air at initial time inside the cylinder with the sample, respectively. $P(t)$ is the sum of remaining initial air pressure (P_o) and time-varying released gas pressure [$\Delta P(t)$] from specimen, i.e., $P(t) = P_o + \Delta P(t)$, n_0 is remaining initial air mole, and $\Delta n(t)$ is the time-varying gas mole corresponding to gas pressure increase by the released gas. $\alpha(t)$ is the change rate of temperature with respect to T_0. Thus, $\Delta n(t)$ is transformed into the released gas concentration [$\Delta C(t)$] per mass for specimen as [86]:

$$\Delta C(t)[\text{wtppm}] = \Delta n(t)[\text{mol}] \times \frac{m_{Gas}\left[\frac{\text{g}}{\text{mol}}\right]}{m_{specimen}[\text{g}]} \times 10^6$$

$$= \frac{V_0}{RT_0}[\Delta P(t) - \alpha(t)P_0 - \alpha(t)\Delta P(t)][\text{mol}] \times \frac{m_g\left[\frac{\text{g}}{\text{mol}}\right]}{m_{specimen}[\text{g}]} \times 10^6 \tag{5}$$

where m_g[g/mol] is molar mass of the gas used; for H_2, m_{H_2} [g/mol] = 2.016 g/mol and for N_2, m_{N_2} [g/mol] = 28.001 g/mol; and $m_{specimen}$ is sample mass. First term, $\Delta P(t)$ in Eq. (5), is the increase in pressure that is emitted gas from sample. The second term, $-\alpha(t)P_0$, is the pressure change caused by temperature variation [$\alpha(t)$]. The third term, $-\alpha(t)\Delta P(t)$, is the pressure change due to both temperature variation [$\alpha(t)$] and pressure increase [$\Delta P(t)$].

According to Eqs. (4) and (5), the time-varying gas mole, $\Delta n(t)$, is transformed to gas mass concentration, [$\Delta C(t)$], by k: $k = \left[\frac{m_g}{m_{specimen}}\right]$. $\Delta n(t)$ and $\Delta C(t)$ are affected by both temperature and pressure variations. Thus, we have compensated for the variations caused by changes in temperature and pressure.

2.4 Analysis Program for Obtaining Transport Parameters

Released gas concentration from the gas-charged sample follows Fickian diffusion. Thus, the concentration of released gas, $C_E(t)$, is calculated as follows [88,89]:

$$C_E(t)/C_\infty = 1 - \frac{32}{\pi^2} \times \left[\Sigma_{n=0}^{\infty} \frac{\exp\left\{\frac{-(2n+1)^2\pi^2 Dt}{l^2}\right\}}{(2n+1)^2}\right] \times \left[\Sigma_{n=1}^{\infty} \frac{\exp\left\{\frac{D\beta_n^2 t}{l^2}\right\}}{\beta_n^2}\right]$$

$$= 1 - \frac{32}{\pi^2} \times \left[\frac{\exp\left(-\frac{\pi^2 Dt}{l^2}\right)}{1^2} + \frac{\exp\left(-\frac{3^2\pi^2 Dt}{l^2}\right)}{3^2} + \cdots, \right.$$

$$\left. + \frac{\exp\left(-\frac{(2n+1)^2\pi^2 Dt}{l^2}\right)}{(2n+1)^2} + \cdots, \right]$$

$$\times \left[\frac{\exp\left(-\frac{D\beta_1^2 t}{\rho^2}\right)}{\beta_1^2} + \frac{\exp\left(-\frac{D\beta_2^2 t}{\rho^2}\right)}{\beta_2^2} + \cdots, + \frac{\exp\left(-\frac{D\beta_n^2 t}{\rho^2}\right)}{\beta_n^2} + \ldots, \right] \tag{6}$$

where β_n represents root of zeroth-order Bessel function, $J_0(\beta_n)$. This equation corresponds to solution of Fick's second diffusion equation for a cylindrical shaped specimen. $C_E(t=0) = 0$ and $C_E(t = ¥) = C_\infty$ is saturated gas concentration at infinite time, indicating total gas uptake (Emission Content). D is the gas diffusivity. l and ρ are thickness and radius of cylindrical sample, respectively.

For the exact calculation by Eq. (6), many terms in the product of two summations are contained. Therefore, dedicated analysis program is developed that calculates precisely C_∞ and D. With an analysis program based on an optimization algorithm [90], we accurately calculate $C_E(t)$ and D from the measured result by solving the Eq. (6).

3. Results and Discussion

3.1 Volumetric Measurement

After decompressing a specimen charged with corresponding gas under high pressure, the released gas concentration and diffusivity

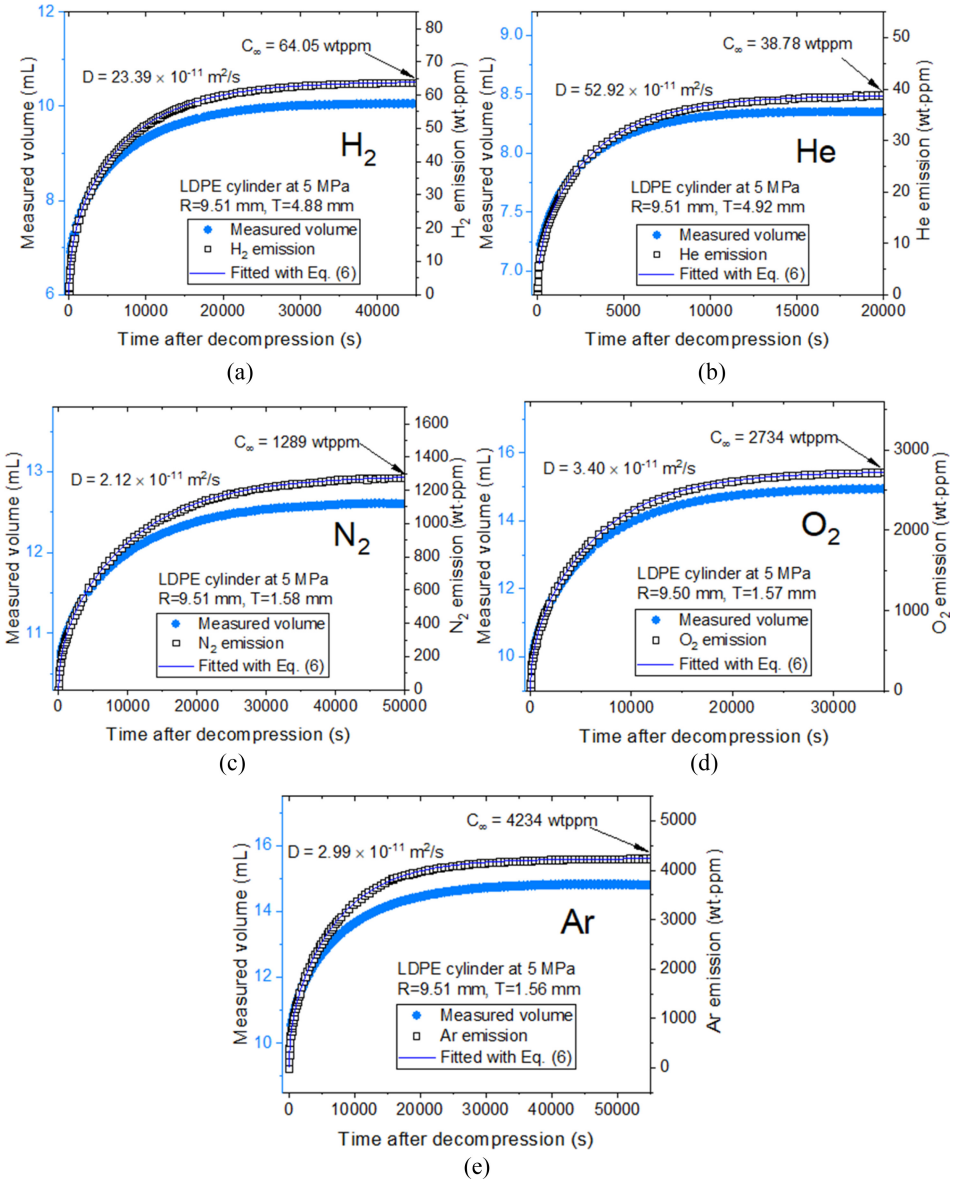

Fig. 3 Gas uptake and diffusivity determined from five gases in a cylindrical LDPE specimen by volumetric measurement using image processing algorithm and a digital camera. (a-e): Measured gas volume (Filled circle) transformed from the measured water level and emitted gas emission (Open square) transferred from measured gas volume in unit of wt·ppm. The fitting line represents the fitted result using Eq. (6). Diffusivity parameters, D and C_∞, is calculated by an analysis program based on Eq. (6). Here, R is radius of cylindrical specimen. T is thickness of cylindrical specimen

were determined using the VM method with a graduated cylinder (Fig. 1). The water level in VM method is measured by employing image processing algorithm and a digital camera [83]. Fig. 3 displays the measured and fitted results for five gases in cylindrical LDPE determined from the water level measurement by VM. The left sides of Figs. 3(a)-3(e) show corresponding emitted gas volume (Filled circle) transferred from water level measurement. The right sides of Figs. 3(a)-3(e) represent corresponding gas emission data (Open square). The diffusion parameters, and C_∞, are derived using an analysis program by Eq. (6). The fitting line in right side is fitted result using Eq. (6), with diffusivity (D) and the total gas uptake (C_∞) marked by an arrow. As shown in Figs. 3(a)-3(e), single mode gas emission behaviors for all gases in LDPE were observed under time depending gas emission measurement. The single-mode gas emission in LDPE results from gas diffusion into the amorphous phase.

3.2 Manometric Measurement

After decompressing a specimen charged with hydrogen under high pressure, the released gas concentration and diffusivity were determined using the MM method for specimen loaded in the cylinder-shaped container (Fig. 2). The water level in MM method

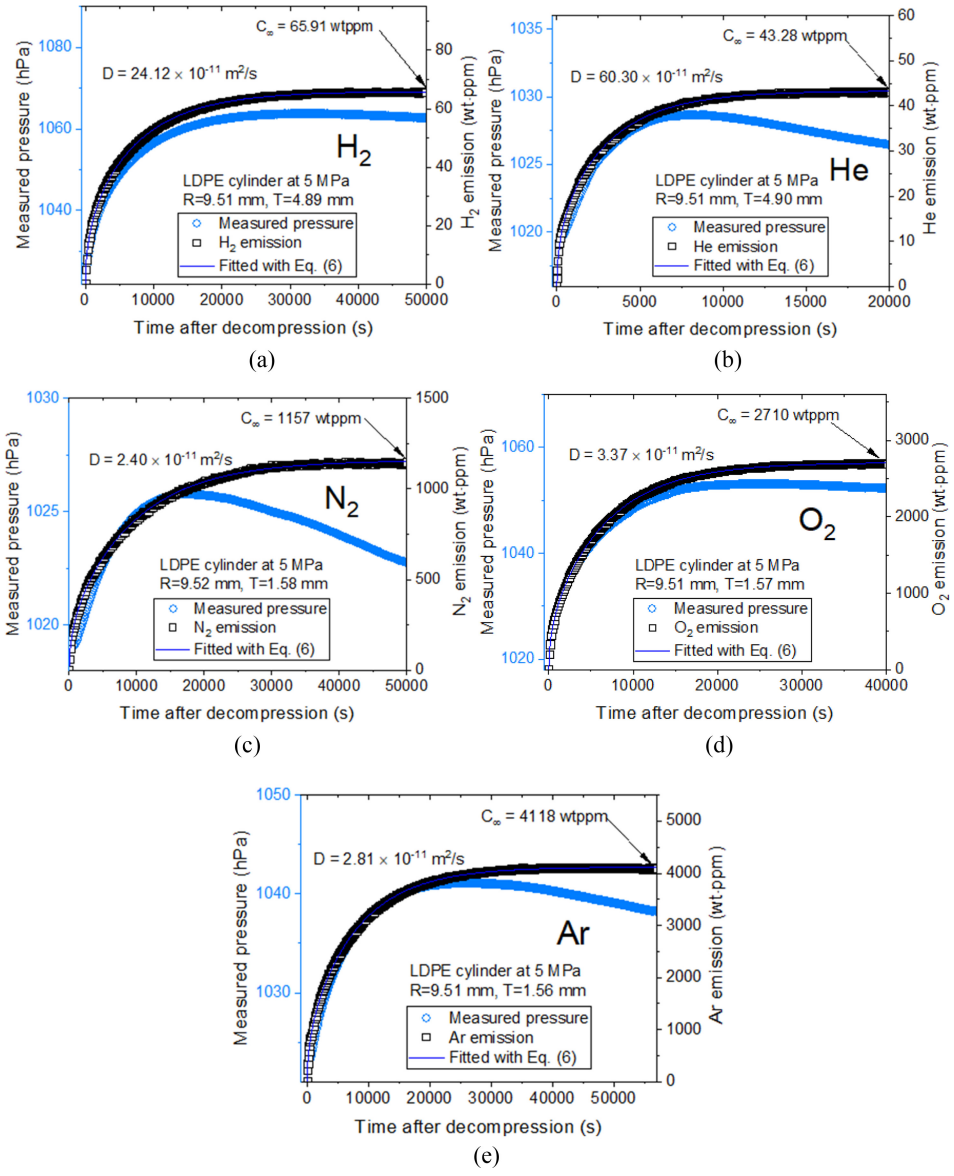

Fig. 4 Gas uptake and diffusivity determined from five gases in a cylindrical LDPE specimen by manometric measurement using data logger. (a-e): Measured gas volume (Filled circle) transformed from the measured water level and emitted gas emission (Open square) transferred from measured gas volume in unit of wt·ppm. The fitting line represents the fitted result using Eq. (6). Diffusivity parameters, D and C_∞, is calculated by an analysis program based on Eq. (6). Here, R is radius of cylindrical specimen. T is thickness of cylindrical specimen

is measured by employing commercial USB-type manometer. Figs. 4(a)-4(e) display the measured and fitted results for five gases in cylindrical LDPE determined from the water level measurement by MM. The left and right sides of Figs. 4(a)-4(e) represent emitted gas volume transferred from water level measurement and gas emission content, respectively. The right sides of Figs. 4(a)-4(e) represent the diffusion parameters, D and C_∞, derived using a diffusion analysis program by Eq. (6). The fitting line in right side is fitted data using Eq. (6), with gas diffusivity and the total gas uptake marked by an arrow. In similarity with Fig. 3, a single-mode gas emission behaviors for all gases in LDPE were also observed under time varying gas emission measurement in Fig. 4.

Moreover, solubility (S) is obtained from gas uptake versus pressure from Figs. 3 and 4 as follows [84,91-93]:

$$S\left[\frac{\text{mol}}{\text{m}^3\cdot\text{MPa}}\right]=\frac{(C_\infty/\text{pressure})\left[\frac{\text{wt}\cdot\text{ppm}}{\text{MPa}}\right]\times 10^6\times d\left[\frac{\text{g}}{\text{m}^3}\right]}{m_g\left[\frac{\text{g}}{\text{mol}}\right]} \quad (7)$$

m_g is molar mass of the charged gas and d is density of the sample. The solubility and diffusivity in two sensors determined for H_2, He, N_2, O_2 and Ar gases in LDPE sample are shown in Tables 1 and 2,

Table 1 Summary for solubility and diffusivity of five gases measured by VM and MM in LDPE

Sensing method	Solubility [mol/m^3·MPa]					Diffusion coefficient [$\times 10^{-11}$ m^2/s]				
	H_2	He	N_2	O_2	Ar	H_2	He	N_2	O_2	Ar
VM	5.83	1.78	8.45	15.69	19.46	23.39	52.92	2.12	3.40	2.99
MM	6.00	1.99	7.58	15.55	18.93	24.12	60.30	2.40	3.37	2.81

Table 2 Performance comparisons for two sensor systems with volumetric and manometric methods

Performance	Volumetric measurement	Manometric measurement
Sensitivity	16.43 [wt·ppm/mL]	11.96 [wt·ppm/hPa]
Resolution [wt·ppm]	0.08	0.12
Stability [%]	0.2	0.2
Measuring range [wt·ppm]	Max. 1,400	Max. 1,500
Response time [s]	~1	~1
FOM [%]	0.4	0.7

respectively.

In Table 1, the solubility and diffusion coefficient in two specimens for two sensors have 10 % relative expanded uncertainty for measured value. The solubility and diffusion coefficient results obtained from both the VM and MM were consistent within the estimated relative uncertainty.

3.3 Performance Comparison between Volumetric and Manometric Gas Sensors

We have evaluated the performance of two gas sensing system using volumetric image sensor and manometric data logger sensor. The results of the performance tests are represented in Table 2, covering sensitivity, resolution, stability, measurable range, response time and figure of merit (FOM). Sensitivity in VM and MM sensor is defined as the mass concentration change relative to the change in measured volume and measured pressure, respectively. The obtained sensitivities were 16.43 wt·ppm/mL for the VM sensor and 11.96 wt·ppm/hPa for the MM sensor. A sensor with higher sensitivity typically provides better resolution. For the VM sensor, the resolution is reflected by the minimum measurable volume of 0.005 mL, corresponding to a mass concentration of 0.08 wt·ppm. For the MM sensor, the resolution is reflected by the minimum measurable pressure of 0.01 hPa, corresponding to a mass concentration of 0.12 wt·ppm. To improve resolution further, it is possible to reduce the inner volume of the graduated cylinder and the sample container or increase the number of specimens. This adjustment would lead to better sensitivity and resolution.

The stability of two sensor systems is quantified by the standard deviation of measurements taken over 36 hours after gas emission from the specimen ceased. This was found to be less than 0.2% of the mass concentration for both sensors. The measurable range in VM sensor is obtained as the maximum allowable concentration per mass of specimen within graduated cylinder with inner volumes. The measurable range in MM sensor is determined as the maximum allowable concentration per mass of specimen within a specimen container with inner volumes. For both the sensors, the measurable range was 1,400 wt·ppm for VM sensor and 1,500 wt·ppm for MM sensor, which can be adjusted by varying the sample mass, cylinder volume and specimen container volume. The gas sensor's volume and pressure response are almost instantaneous, occurring within ~1 second of gas emission. The figure of merit (FOM) is defined as the standard deviation between measured data and the theoretical value calculated using Eq. (3). An FOM value is below 0.4% for VM sensor and 0.7% for MM sensor, indicating good agreement between the measured and theoretical values. Based on the performance testing, the specifications (Sensitivity, Resolution and FOM) of VM sensor are superior to MM sensor.

4. Conclusion

Gas sensors are crucial for ensuring safety and protecting property in gas-related facilities. We have developed two gas sensing systems that utilize volumetric measurements with a graduated cylinder, coupled with an image processing algorithm and a digital camera. The variation in the water level, observed through pixel shifts in the graduated cylinder, is directly linked to changes in water volume caused by the released gas, allowing for precise measurement of gas concentration. By integrating a

diffusion-permeation analysis program, this volumetric image-based gas sensor is capable of detecting not only gas concentrations but also solubility/diffusivity from gas-charged specimens under high-pressure conditions.

A straightforward manometric gas sensor was also developed for characterizing gas behavior. The method relies on pressure measurements within a gas charged sample container, utilizing a commercial data logger. The system measures the pressure increase caused by the gas released from high-pressure polymer samples, enabling the determination of gas concentration and solubility/diffusivity by a diffusion analysis program.

The two portable gas sensor systems showcased several key performance metrics: a low detection limit for gas content, a measurable range of up to 1,500 wt·ppm, stability of 0.2%, and a rapid response time within one second. Additionally, the sensors' insensitivity to temperature and pressure fluctuations made them highly reliable for gas detection. The sensing systems, utilizing both volumetric and manometric measurements, successfully demonstrated real-time monitoring and characterization of pure gases such as H_2, He, N_2, O_2 and Ar. The sensors effectively measured gas uptake and diffusivity, considering influencing factors and calculating expanded uncertainty. In conclusion, the main features of the two developed gas sensing methods are summarized as follows:

- **Cost-effective and simple techniques**: The two methods provide affordable and straightforward solutions for evaluating gas uptake and diffusion coefficient in gas charged polymers under high-pressure.
- **Stability against temperature and pressure variations**: Both methods are stable under fluctuations in temperature and pressure. Two sensors are independent on a specimen sizes, shapes and gas types.
- **Adjustable sensitivity and range**: The volumetric and manometric methods offer flexible sensitivity, resolution, and measurement range, allowing for customization based on specific application requirements.
- **No chemical interaction**: Both sensing methods function without any interaction between the gas molecules and the sensor, ensuring accurate measurements without altering the composition of the gas.
- **Visible gas release monitoring:** The volumetric method provides visual gas monitoring of gas release by changes in water level.

These two complementary sensing methods are highly effective for measuring gas transport properties in sealing elastomers and can be applied to assess the permeation characteristics of rubber materials and O-rings under high-pressure conditions. They are particularly well-suited for applications in hydrogen fueling stations. The results from both sensing methods demonstrated consistent measurements of gas solubility and diffusivity, with a comprehensive review of their characteristics and performance, ensuring their reliability and applicability in the field.

REFERENCES

1. Wang, Z., Zhu, L., Zhang, J., Wang, J., Cui, X., Chen, X., Liu, W., Ma, H., Wang, J., Yan, W., (2024), ZIF-8 loaded Ag/ZnO electrospun nanofibers enabling high-performance H_2 gas sensing for battery safety early warning, Sensors and Actuators B: Chemical, 418, 136276.
2. Murthy, H., (2024), Complex and composite metal oxides for gas, VOC, and humidity sensors, In: Yadav, B. C., Kumar, P. (Eds.), Elsevier, 133-157.
3. Jung, J. K., Kim, I. G., Chung, K. S., Baek, U. B., (2021), Analyses of permeation characteristics of hydrogen in nitrile butadiene rubber using gas chromatography, Materials Chemistry and Physics, 267, 124653.
4. Jung, J. K., Lee, J. H., (2024), High-performance hydrogen gas sensor system based on transparent coaxial cylinder capacitive electrodes and a volumetric analysis technique, Scientific Reports, 14(1), 1967.
5. Li, J., Li, Y., Zeng, W., (2024), Gas sensing technology as the key to safety warning of lithium-ion battery: Recent advance, Sensors and Actuators A: Physical, 365, 114890.
6. Yang, Y., Zheng, S., Fu, X., Zhang, H., (2018), Remote and portable mechanoluminescence sensing system based on a $SrAl_2O_4$:Eu,Dy film and its potential application to stress sensing in flexible structures, Optik, 158, 602-609.
7. Mohapatra, P., Panigrahi, S., Amamcharla, J., (2015), Evaluation of a commercial electronic nose system coupled with universal gas sensing chamber for sensing indicator compounds associated with meat safety, Journal of Food Measurement and Characterization, 9, 121-129.
8. Wenger, M., Waller, R., Lorentz, V. R. H., Marz, M., Herold, M., (2014), A novel approach for online condition monitoring of power transformers using frequency response analysis, Proceedings of the IECON 2014 - 40th Annual Conference of the IEEE Industrial Electronics Society, 5654-5659.
9. Kang, H. M., Choi, M. C., Lee, J. H., Yun, Y. M., Jang, J. S., Chung, N. K., Jeon, S. K., Jung, J. K., Lee, J. H., Lee, J. H., Chang, Y. W., Bae, J. W., (2022), Effect of the high-pressure hydrogen gas exposure in the silica-filled EPDM sealing composites with different silica content, Polymers, 14(6), 1151.
10. Jung, J. K., Kim, I. G., Kim, K. T., (2021), Evaluation of hydrogen permeation characteristics in rubbery polymers, Current Applied Physics, 21, 43-49.

11. Sony, A., Acharjya, K., Sharma, K., Beemkumar, N., (2024), Production of green hydrogen through renewable energy sources based microgrid, Proceedings of the E3S Web of Conferences, 540, 11001.

12. Kayacık, S. E., Schrotenboer, A. H., Ursavas, E., Vis, I. F., (2024), Towards low-carbon power networks: Optimal location and sizing of renewables energy sources and hydrogen storage, Sustainable Energy, Grids and Networks, 38, 101394.

13. Amez, I., Castells, B., León, D., Paredes, R., (2025), Study of quaternary hydrogen and biogas mixtures: An industrial safety approach, Fuel, 381, 133663.

14. Wu, M., Bai, L., Deng, F., He, J., Song, K., Li, H., (2025), Organic-inorganic hybrid materials for catalytic transfer hydrogenation of biomass-derived carbonyl compounds, Coordination Chemistry Reviews, 523, 216259.

15. Tang, M., Qin, C., Sun, X., Li, M., Wang, Y., Cao, J., Wang, Y., (2024), Enhanced H_2 gas sensing performances by Pd-loaded In_2O_3 microspheres, Applied Physics A, 130(10), 741.

16. Jung, J. K., Kim, I. G., Kim, K.-T., Baek, U. B., Nahm, S. H., (2021), Novel volumetric analysis technique for characterizing the solubility and diffusivity of hydrogen in rubbers, Current Applied Physics, 26, 9-15.

17. Tom, A., Singh, D. K., Shaw, V. K., Abhijith, P. V., Sajana, S., Kirandas, P. S., Dixit, V., Kamble, V., Pai, S. P., Jaiswal-Nagar, D., (2024), Feedback-based gas sensing setup for ppb to ppm level sensing, Review of Scientific Instruments, 95(8), 085003.

18. Venkatesan, R., Harun, R., Yusoff, H. M., Razak, M. A., (2024), Hydrogen safety effect calculation (dispersion and thermal radiation effects) for determination of siting and safe distance, Process Safety Progress, 43, S161-S169.

19. Malik, A. A., Rusli, R., Nazir, S., Wong, R. H., Arshad, U., (2024), Grid-based assessment of hydrogen leakages for an offshore process to improve the design and human performance, Process Safety Progress, 43, S35-S49.

20. Lu, J. N., Huang, Y., Xia, Y. S., Dong, L. Z., Zhang, L., Liu, J. J., Xie, L. G., Liu, J., Lan, Y. Q., (2024), Selective photosynthesis of Z-olefins through crystalline metal–organic cage-initiated expeditious cascade reactions, Carbon Energy, 6(3), e396.

21. Kang, H., Bae, J., Lee, J., Yun, Y., Jeon, S., Chung, N., Jung, J., Baek, U., Lee, J., Kim, Y., Choi, M., (2024), The synergistic effect of carbon black/carbon nanotube hybrid fillers on the physical and mechanical properties of EPDM composites after exposure to high-pressure hydrogen gas, Polymers, 16(8), 1065.

22. Jung, J. K., Kim, K. T., Chung, N. K., Baek, U. B., Nahm, S. H., (2022), Characterizing the diffusion property of hydrogen sorption and desorption processes in several spherical-shaped polymers, Polymers, 14(7), 1468.

23. Wang, Y., Pang, Y., Xu, H., Martinez, A., Chen, K. S., (2022), PEM fuel cell and electrolysis cell technologies and hydrogen infrastructure development – A review, Energy & Environmental Science, 15(6), 2288-2328.

24. Fujiwara, H., Ono, H., Onoue, K., Nishimura, S., (2020), High-pressure gaseous hydrogen permeation test method - Property of polymeric materials for high-pressure hydrogen devices (1), International Journal of Hydrogen Energy, 45(53), 29082-29094.

25. Fujisawa, A., Kinoshita, S., Miura, S.-I., Nakao, S., Suzuki, F., Yamashita, K., (2020), Demonstration of hydrogen refueling station using renewable energy for fuel cell vehicles, Kobelco Tehcnology Review, 70(39), 1-5.

26. Jung, J. K., Moon, Y. I., Chung, K. S., Kim, K. T., (2020), Development of a program for analyzing dielectric relaxation and its application to polymers: Nitrile butadiene rubber, Macromolecular Research, 28, 596-604.

27. Jang, J. S., Chung, N. K., (2020), Measurement of the hydrogen permeability of various polymers for high pressure hydrogen storage vessels and valves, Proceedings of the ASME Pressure Vessels and Piping Conference, Volume 1: Codes and Standards, American Society of Mechanical Engineers, V001T01A041.

28. Profatilova, I., Fouda-Onana, F., Heitzmann, M., Bacquart, T., Morris, A., Warren, J., Haloua, F., Jacques, P.-A., (2024), Detrimental impact of trace amount of tetrachlorohexafluorobutane impurity in hydrogen on PEM fuel cell performance, International Journal of Hydrogen Energy, 65, 837-849.

29. Menon, N. C., Kruizenga, A. M., Alvine, K. J., San Marchi, C., Nissen, A., Brooks, K., (2016), Behavior of polymers in high-pressure environments as applicable to the hydrogen infrastructure, Proceedings of the ASME Pressure Vessels and Piping Conference 2016, Volume 6B: Materials and Fabrication, American Society of Mechanical Engineers, PVP2016-63713.

30. Moon, Y. I., Jung, J. K., Kim, G. H., Chung, K. S., (2021), Observation of the relaxation process in fluoroelastomers by dielectric relaxation spectroscopy, Physica B: Condensed Matter, 608, 412870.

31. Zhanguo, S. U., Zhang, W., Abdulwahab, A., Saleem, S., Yao, Y., Deifalla, A., Taghavi, M., (2023), Comparison of gasoline and hydrogen pathways in order to reduce the environmental hazards of a solar-hydrogen refueling station: Evaluation based on life cycle cost and well-to-wheel models, Process Safety and Environmental Protection, 173, 317-331.

32. Jung, J. K., Lee, J. H., Jeon, S. K., Baek, U. B., Lee, S. H., Lee, C. H., Moon, W. J., (2023), H_2 uptake and diffusion characteristics in sulfur-crosslinked ethylene propylene diene monomer polymer composites with carbon black and silica fillers after high-pressure hydrogen exposure reaching 90 MPa, Polymers, 15(1), 162.

33. Jung, J. K., Baek, U. B., Lee, S. H., Choi, M. C., Bae, J. W., (2023), Hydrogen gas permeation in peroxide-crosslinked ethylene propylene diene monomer polymer composites with carbon black and silica fillers, Journal of Polymer Science, 61(6), 460-471.

34. Choi, B. L., Jung, J. K., Baek, U. B., Choi, B. H., (2022), Effect of functional fillers on tribological characteristics of acrylonitrile butadiene rubber after high-pressure hydrogen exposures, Polymers, 14(5), 861.

35. Lee, C. H., Jung, J. K., Jeon, S. K., Ryu, K. S., Baek, U. B., (2017), Nuclear magnetic resonance study of O-ring polymer exposed to high-pressure hydrogen, Journal of Magnetics, 22(3), 478-482.

36. Flamm, B., Peter, C., Büchi, F. N., Lygeros, J., (2021), Electrolyzer modeling and real-time control for optimized production of hydrogen gas, Applied Energy, 281, 116031.

37. Kuang, W., Bennett, W. D., Roosendaal, T. J., Arey, B. W., Dohnalkova, A., Petrossian, G., Simmons, K. L., (2021), In situ friction and wear behavior of rubber materials incorporating various fillers and/or a plasticizer in high-pressure hydrogen, Tribology International, 153, 106627.

38. Lee, J. H., Kim, Y. W., Jung, J. K., (2023), Investigation of the gas permeation properties using the volumetric analysis technique for polyethylene materials enriched with pure gases under high pressure: H_2, He, N_2, O_2 and Ar, Polymers, 15(19), 4019.

39. Lee, J. H., Kim, Y. W., Kim, D. J., Chung, N. K., Jung, J. K., (2024), Comparison of two methods for measuring the temperature dependence of H_2 permeation parameters in nitrile butadiene rubber polymer composites blended with fillers: The volumetric analysis method and the differential pressure method, Polymers, 16(2), 280.

40. Lee, J. H., Kim, Y. W., Chung, N. K., Kang, H. M., Moon, W. J., Choi, M. C., Jung, J. K., (2024), Multiphase modeling of pressure-dependent hydrogen diffusivity in fractal porous structures of acrylonitrile butadiene rubber-carbon black composites with different fillers, Polymer, 311, 127552.

41. Lee, C. H., Jung, J. K., Kim, K. S., Kim, C. J., (2024), Hierarchical channel morphology in O-rings after two cycling exposures to 70 MPa hydrogen gas: A case study of sealing failure, Scientific Reports, 14(1), 5319.

42. Jung, J. K., Lee, J. H., Jang, J. S., Chung, N. K., Park, C. Y., Baek, U. B., Nahm, S. H., (2022), Characterization technique of gases permeation properties in polymers: H_2, He, N_2 and Ar gas, Scientific Reports, 12(1), 3328.

43. Moon, Y., Lee, H., Jung, J., Han, H., (2023), Direct visualization of carbon black aggregates in nitrile butadiene rubber by THz near-field microscope, Scientific Reports, 13(1), 7846.

44. Kim, G. H., Moon, Y. I., Jung, J. K., Choi, M. C., Bae, J. W., (2022), Influence of carbon black and silica fillers with different concentrations on dielectric relaxation in nitrile butadiene rubber investigated by impedance spectroscopy, Polymers, 14(1), 155.

45. Jung, J. K., Lee, C. H., Baek, U. B., Choi, M. C., Bae, J. W., (2022), Filler influence on H_2 permeation properties in sulfur-crosslinked ethylene propylene diene monomer polymers blended with different concentrations of carbon black and silica fillers, Polymers, 14(3), 592.

46. Liu, C., Zhang, R., Tian, L., Pei, Y., Li, Y., (2022), Research progress on compatibility of non-metallic pipes in hydrogen environment, Natural Gas Industry, 42(9), 145-156.

47. Smith, D. B., Frame, B. J., Anovitz, L. M., Makselon, C., (2016), Feasibility of using glass-fiber-reinforced polymer pipelines for hydrogen delivery, Proceedings of the ASME Pressure Vessels and Piping Conference 2016, 6B: Materials and Fabrication, American Society of Mechanical Engineers, V06BT06A036.

48. Chou, Y. S., Stevenson, J. W., (2009), Long-term ageing and materials degradation of hybrid mica compressive seals for solid oxide fuel cells, Journal of Power Sources, 191(2), 384-389.

49. Li, G., Zhang, J., Chai, J., Ni, Z., Yan, Y., (2024), Cryogenic mechanical performance and gas-barrier property of epoxy resins modified with multi-walled carbon nanotubes, International Journal of Hydrogen Energy, 89, 738-745.

50. Yuan, S., Zhang, S., Wei, J., Gao, Y., Zhu, Y., Wang, H., (2024), Materials selection, design, and regulation of polymer-based hydrogen barrier composite coatings, membranes and films for effective hydrogen storage and transportation: A comprehensive review, International Journal of Hydrogen Energy, 91, 555-573.

51. Jeon, S. K., Jung, J. K., Chung, N. K., Baek, U. B., Nahm, S. H., (2022), Investigation of physical and mechanical characteristics of rubber materials exposed to high-pressure hydrogen, Polymers, 14(11), 2233.

52. Theiler, G., Murillo, N. C., Hausberger, A., (2024), Effect of hydrogen pressure on the fretting behavior of rubber materials, Lubricants, 12(7), 233.

53. Checchetto, R., Scarpa, M., De Angelis, M. G., Minelli, M., (2022), Mixed gas diffusion and permeation of ternary and quaternary $CO_2/CO/N_2/O_2$ gas mixtures in Matrimid®, polyetherimide and poly(lactic acid) membranes for CO_2/CO separation, Journal of Membrane Science, 659, 120768.

54. Pavani, G. J., Pavani, S. A., Ferreira, C. A., (2021), Gas permeameter in polymer nanocomposite plates: Construction and validation, Iranian Polymer Journal, 30(6), 583-591.

55. Brown, D., Neyertz, S., Raaijmakers, M. J. T., Benes, N. E., (2019), Sorption and permeation of gases in hyper-cross-linked hybrid poly(POSS-imide) networks: An in silico study, Journal of Membrane Science, 577, 113-128.

56. Sun, G., Wang, C., Jia, J., Zhang, H., Hu, Y., Liu, Y., Zhang, D., (2024), High-performance ammonia detection of polymeric $BaTiO_3/Ti_3C_2T_x$ MXene composite-based sensor for gas emission and leakage, Journal of Electronic Materials, 53(7), 3426-3435.

57. Lo, J.-H., Smits, K. M., Cho, Y., Duggan, G. P., Riddick, S. N., (2024), Quantifying non-steady state natural gas leakage from the pipelines using an innovative sensor network and model for subsurface emissions - InSENSE, Environmental Pollution, 341, 122810.

58. Sadovnikov, S. A., Yakovlev, S. V., Kravtsova, N. S., Romanovskii, O. A., Tuzhilkin, D. A., (2025), Dual-channel infrared OPO lidar optical system for remote sensing of greenhouse gases in the atmosphere: Design and characteristics, Sensors International, 6, 100307.

59. Meng, J., Balendhran, S., Sabri, Y., Bhargava, S. K., Crozier, K. B., (2024), Smart mid-infrared metasurface microspectrometer gas sensing system, Microsystems & Nanoengineering, 10(1), 74.

60. Schlicke, H., Maletz, R., Dornack, C., Fery, A., (2024), Plasmonic particle integration into near-infrared photodetectors and photoactivated gas sensors: Toward sustainable next-generation ubiquitous sensing, Small, 20(48), 2403502.

61. Molleman, B., Alessi, E., Passaniti, F., Daly, K., (2024), Evaluation of the applicability of a metal oxide semiconductor gas sensor for methane emissions from agriculture, Information Processing in Agriculture, 11(4), 573-580.

62. Kwon, S.-K., Kim, J.-N., Byun, H.-G., Kim, H.-J., (2024), Low-power and cost-effective readout circuit design for compact semiconductor gas sensor systems, Electrochemistry Communications, 169, 107834.

63. Eshkobilova, M., Smanova, Z., Begimqulov, J., Suvankulov, S., Abdurakhmanov, E., (2024), Template synthesis of gas-sensitive nanocomposite thin surfaces based on metal oxides for natural gas detection semiconductor sensors, AIP Conference Proceedings, 3244, 050007.

64. Zhang, X., Ojha, B., Bichlmaier, H., Hartmann, I., Kohler, H., (2023), Extensive gaseous emissions reduction of firewood-fueled low power fireplaces by a gas sensor based advanced combustion airflow control system and catalytic post-oxidation, Sensors, 23(10), 4679.

65. Rodlamul, P., Tamura, S., Imanaka, N., (2019), Effect of p- or n-type semiconductor on CO sensing performance of catalytic combustion-type CO gas sensor with CeO_2-ZrO_2-ZnO based catalyst, Bulletin of the Chemical Society of Japan, 92(3), 585-591.

66. Jang, W., Park, J.-S., Lee, K.-W., Roh, Y., (2018), Methane and hydrogen sensing properties of catalytic combustion type single-chip micro gas sensors with two different Pt film thicknesses for heaters, Micro and Nano Systems Letters, 6, 1-5.

67. Xie, R., Guan, S., Tan, Z., (2025), A gas sensor scheme for CO based on optical-feedback linear-cavity enhanced absorption spectroscopy, Optics Communications, 574, 131105.

68. Zhang, Y., Wang, M., Yu, P., Liu, Z., (2022), Optical gas-cell dynamic adsorption in a photoacoustic spectroscopy-based SOF_2 and SO_2F_2 gas sensor, Sensors, 22(20), 7949.

69. Yarai, A., Nakanishi, T., (2004), Optical fiber gas sensor based on thermal lens spectroscopy, Review of Scientific Instruments, 75(10), 3237-3241.

70. Seleka, W. M., Ramohlola, K. E., Modibane, K. D., Makhado, E., (2024), Conductive chitosan/polyaniline hydrogel: A gas sensor for room-temperature electrochemical hydrogen sensing, International Journal of Hydrogen Energy, 68, 940-954.

71. Mishra, S. R., Gadore, V., Ahmaruzzaman, M., (2024), Recent advances in In_2S_3-based nanocomposites for gas and electrochemical sensors: Mechanisms and developments, Materials Letters, 359(19), 135946.

72. Asilian, A., Zanjani, S. M., (2024), Application of levenberg-marquardt backpropagation algorithm in artificial neural network for self-calibration of deflection type wheatstone bridge circuit in co electrochemical gas sensor, Majlesi Journal of Electrical Engineering, 18(1), 21-32.

73. Jung, J. K., Kim, I. G., Chung, K. S., Kim, Y.-I., Kim, D. H., (2021), Determination of permeation properties of hydrogen gas in sealing rubbers using thermal desorption analysis gas chromatography, Scientific Reports, 11(1), 17092.

74. Jung, J. K., Kim, I. G., Chung, K. S., Baek, U. B., (2021), Gas chromatography techniques to evaluate the hydrogen permeation characteristics in rubber: Ethylene propylene diene monomer, Scientific Reports, 11(1), 4859.

75. Jung, J. K., Kim, K.-T., Chung, K. S., (2022), Two volumetric techniques for determining the transport properties of hydrogen gas in polymer, Materials Chemistry and Physics, 276, 125364.

76. Jung, J. K., Kim, I. G., Kim, K. T., Ryu, K. S., Chung, K. S., (2021), Evaluation techniques of hydrogen permeation in sealing rubber materials, Polymer Testing, 93, 107016.

77. Hardoyono, F., Windhani, K., (2023), Combination of metal oxide semiconductor gas sensor array and solid-phase microextraction gas chromatography–mass spectrometry for odour classification of brewed coffee, Flavour and Fragrance Journal, 38(6), 451-463.

78. Huang, Z., Yang, W., Zhang, Y., Yin, J., Sun, X., Sun, J., Ren, G., Tian, S., Wang, P., Wan, H., (2024), Miniaturized electrochemical gas sensor with a functional nanocomposite and thin ionic liquid interface for highly sensitive and rapid detection of hydrogen, Analytical Chemistry, 96(45), 17960-17968.

79. Hinojo, A., Lujan, E., Abella, J., Colominas, S., (2024), Development and characterization of electrochemical hydrogen sensors using different fabrication techniques, Fusion Engineering and Design, 204, 114483.

80. Jung, J. K., Kim, I. G., Jeon, S. K., Chung, K. S., (2021), Characterizing the hydrogen transport properties of rubbery polymers by gravimetric analysis, Rubber Chemistry and Technology, 94(4), 688-703.

81. Zhu, X., Ahmed, W., Schmidt, K., Barroso, R., Fowler, S. J., Blanford, C. F., (2024), Validation of an electronic VOC sensor against gas chromatography-mass spectrometry, IEEE Transactions on Instrumentation and Measurement, 73(1).

82. Shaltaeva, Y. R., Podlepetsky, B. I., Pershenkov, V. S., (2017), Detection of gas traces using semiconductor sensors, ion mobility spectrometry, and mass spectrometry, European Journal of Mass Spectrometry, 23(4), 217-224.

83. Lee, J. H., Jung, J. K., (2024), Development of image-based water level sensor with high-resolution and low-cost using image processing algorithm: Application to outgassing measurements from gas-enriched polymer, Sensors, 24(23), 7699.

84. Jung, J. K., Kim, I. G., Jeon, S. K., Kim, K.-T., Baek, U. B., Nahm, S. H., (2021), Volumetric analysis technique for analyzing

the transport properties of hydrogen gas in cylindrical-shaped rubbery polymers, Polymer Testing, 99, 107147.

85. Jung, J. K., Lee, J. H., Jeon, S. K., Tak, N. H., Chung, N. K., Baek, U. B., Lee, S. H., Lee, C. H., Choi, M. C., Kang, H. M., Bae, J. W., Moon, W. J., (2023), Correlations between H_2 permeation and physical/mechanical properties in ethylene propylene diene monomer polymers blended with carbon black and silica fillers, International Journal of Molecular Sciences, 24(3), 2865.
86. Jung, J. K., Kim, K.-T., Baek, U. B., (2022), Simultaneous three-channel measurements of hydrogen diffusion with light intensity analysis of images by employing webcam, Current Applied Physics, 37, 19-26.
87. Jung, J. K., (2024), Review of developed methods for measuring gas uptake and diffusivity in polymers enriched by pure gas under high pressure, Polymers, 16(5), 723.
88. Crank, J., (1979), The mathematics of diffusion, Oxford: Clarendon Press.
89. Demarez, A., Hock, A. G., Meunier, F. A., (1954), Diffusion of hydrogen in mild steel, Acta Metallurgica, 2(2), 214-223.
90. Nelder, J. A., Mead, R., (1965), A simplex method for function minimization, The Computer Journal, 7(4), 308-313.
91. Jung, J. K., Lee, J. H., Kim, Y. W., Chung, N. K., (2024), Development of portable gas sensing system for measuring gas emission concentration and diffusivity using commercial manometric sensors in gas exposed polymers: Application to pure gases, H_2, He, N_2, O_2 and Ar, Sensors and Actuators B: Chemical, 418, 136240.
92. Jung, J. K., Lee, C. H., Son, M. S., Lee, J. H., Baek, U. B., Chung, K. S., Choi, M. C., Bae, J. W., (2022), Filler effects on H_2 diffusion behavior in nitrile butadiene rubber blended with carbon black and silica fillers of different concentrations, Polymers, 14(4), 700.
93. Jung, J. K., Kim, K. T., Baek, U. B., Nahm, S. H., (2022), Volume dependence of hydrogen diffusion for sorption and desorption processes in cylindrical-shaped polymers, Polymers, 14(4), 756.

Ji Hun Lee
Ph.D. candidate in Korea Research Institute of Standards and Science (KRISS). His research interest is polymer materials in hydrogen energy.
E-mail: ljh93@kriss.re.kr

Sang Koo Jeon
Senior researcher in Korea Research Institute of Standards and Science (KRISS). His research interest is polymer materials in hydrogen energy.
E-mail: sangku39@kriss.re.kr